

Robust difference imaging of high surface brightness targets

E. Kerins,¹ M.J. Darnley,² J.P. Duke,² A. Gould,³ C. Han,⁴ A. Newsam,²
B.-G. Park⁵ and R. Street⁶

¹*Jodrell Bank Centre for Astrophysics, School of Physics & Astronomy, University of Manchester, Oxford Road, Manchester M13 9PL*

²*Astrophysics Research Institute, Liverpool John Moores University, Twelve Quays House, Egerton Wharf, Birkenhead, Merseyside CH41 1LD*

³*Department of Astronomy, Ohio State University, 140 West 18th Avenue, Columbus, OH 43210, USA*

⁴*Department of Physics, Chungbuk National University, Chongju 361-763, Korea*

⁵*Korea Astronomy and Space Science Institute, Hwaam-Dong, Yuseong-Gu, Daejeon 305-348, Korea*

⁶*Las Cumbres Observatory Global Telescope Network, 6740 Cortona Drive, Suite 102, Goleta, CA 93117, USA*

28 March 2019

ABSTRACT

Over the last two decades the Andromeda Galaxy (M31) has been something of a test-bed for methods aimed at obtaining accurate time-domain relative photometry within highly crowded fields. Difference imaging methods, originally pioneered towards M31, have evolved into sophisticated methods, such as the Optimal Image Subtraction (OIS) method of Alard & Lupton (1998), that today are most widely used to survey variable stars, transients and microlensing events in our own Galaxy. We show that modern difference image (DIA) algorithms such as OIS, whilst spectacularly successful towards the Milky Way bulge, may perform badly towards high surface brightness targets such as the M31 bulge. Poor results typically occur in the presence of common data systematics that scale with image flux such as internal reflections, scattered light, flat field errors or fringing. Using data from the Angstrom Project microlensing survey of the M31 bulge, we show that very good results are usually obtainable by first performing careful photometric alignment prior to using OIS to perform point-spread function (PSF) matching. This separation of background matching and PSF matching, a common feature of earlier M31 photometry techniques, allows us to take full advantage of the powerful PSF matching flexibility offered by OIS towards high surface brightness targets. We find that difference images produced this way have noise distributions close to Gaussian, showing significant improvement upon results achieved using OIS alone. We show that with this correction light-curves of variable stars and transients can be recovered to within ~ 10 arcseconds of the M31 nucleus. Our method is simple to implement and is quick enough to be incorporated within real-time DIA pipelines. We also demonstrate that OIS is remarkably robust even when, as in the case of the central regions of the M31 bulge, the sky density of variable sources approaches the confusion limit.

Key words: galaxies: individual (M31) – techniques: image processing – techniques: photometric

1 INTRODUCTION

Difference Image Analysis (DIA) is now used routinely to provide very accurate relative photometry of variable stars, transient objects and microlensing events in the Milky Way and other nearby galaxies (Wozniak 2008). DIA permits very accurate relative photometry even within extremely dense stellar fields where conventional photometric methods can fail or suffer from serious bias.

Most DIA pipelines currently in use derive from the Optimal Image Subtraction (OIS) algorithm of Alard & Lupton (1998) and Alard (2000). The OIS algorithm has found widest use in providing accurate relative photometry of stars in the Milky Way and the Magellanic Clouds. Similar schemes that pre-date OIS were originally employed to look for microlensing towards the Andromeda

Galaxy (Tomaney & Crotts 1996; Ansari et al. 1997). Since the stars in the Andromeda Galaxy (M31) are two orders of magnitude further away than those typically monitored in our Galaxy, difference imaging towards M31 throws up several additional challenges to the standard technique.

In this paper we show that towards the bulge of M31, and similarly towards other targets where diffuse background surface brightness dominates the total flux, DIA pipelines based on the OIS algorithm can often yield sub-optimal results due to common image systematics such as internal reflections, scattered light, flat-field errors or fringe effects. Systematics, which may appear at a low level ($\sim 1\%$) on the original exposures, can give rise to large-amplitude differential background residuals on difference image frames. Since OIS minimizes mismatches in both the point

spread function (PSF) and the differential background simultaneously, poor background matching often results in poor PSF matching and therefore substantial systematic errors in differential photometry. We propose a straightforward remedy to allow the effects of such systematics to be minimized.

The structure of the paper is as follows. In Section 2 we briefly describe how M31 has been used as a test-bed in developing time-domain photometry towards crowded stellar fields. The evolution of these methods culminated in the Optimal Image Subtraction (OIS) algorithm of Alard & Lupton (1998) and Alard (2000), which forms the basis for most DIA pipelines currently in use. We use images obtained by the Angstrom Project (Kerins et al. 2006) of the bulge region of M31 to show how the OIS algorithm may not perform optimally in the presence of bright backgrounds. In Section 3 we show how difference images with noise levels close to the photon noise limit can be recovered by separating the photometric alignment and PSF matching stages. In Section 4 we illustrate how our method minimizes the worst effects of scattered light. We also show that DIA results are remarkably robust even when the sky density of variable sources approaches the confusion limit. We discuss the findings in Section 5.

2 DIFFERENCE IMAGING TOWARDS THE M31 BULGE

2.1 Relative photometry in very crowded fields

The Andromeda Galaxy has provided something of a test-bed for the development of algorithms designed to obtain accurate relative photometry within crowded fields. At around the same time two techniques emerged, difference imaging (Tomaney & Crotts 1996) and super-pixel photometry (Ansari et al. 1997). Both techniques deal with the difficulty of obtaining robust relative photometry across epochs in the presence of variations in seeing and sky background.

Tomaney & Crotts (1996) advocated the difference imaging approach, in which they convolve a high quality reference image with a Gaussian kernel to match the point spread function (PSF) of a target image. Prior to the convolution step the smooth M31 background light was subtracted from both images using unsharp masking. This approach formed the basis of most current difference imaging codes, though it assumes the basic functional form of the PSF is known a priori.

In the super-pixels method (Ansari et al. 1997) an image pair was also photometrically aligned in order to match the background levels. This was done first through linear photometric alignment and then by local median filtering the images to produce smooth background maps. The background map was subtracted from the target image and replaced with that of the reference image. In the absence of seeing variations, or intrinsic source variability, the distribution of image flux deviations (measured within square pixel arrays, or super-pixels) with respect to the local background flux should be statistically the same between aligned image pairs. By plotting the two distributions against one another and determining the best linear fit, a simple linear flux correction can be made to the target image flux to correct for seeing changes. The super-pixels technique has the advantage of being empirically calibrated, avoiding strong assumptions on the form of the PSF. However in principle it is not as sensitive as difference imaging due to the potential loss of signal through binning flux into super-pixels.

Interestingly both of these methods separate out the background correction from the seeing correction. Modern difference

imaging algorithms make these two corrections simultaneously. Whilst this is a highly efficient approach, as we shall show, it does not always yield optimal results.

2.2 Optimal image subtraction

Most difference image packages currently in use employ the Optimal Image Subtraction (OIS) algorithm presented by Alard & Lupton (1998) and generalized further by Alard (2000). In the OIS method a reference image R is convolved to match the PSF of a target image T that has been geometrically aligned and re-sampled to the same pixel grid as R . By taking into account differences in the background between R and T via a smooth 2D background model, B , the difference image, D , can be computed from linear least-squares minimization:

$$\sum_i D(x_i, y_i)^2 = \min\left\{\sum_i [(R(x_i, y_i) \otimes K(u, v)) - T(x_i, y_i) + B(x_i, y_i)]^2\right\} \quad (1)$$

where (x, y) denote the position of image pixel i , K is a kernel function that describes the PSF transformation between R and T , (u, v) are coordinates centred on the kernel and \otimes denotes convolution. For computational efficiency Alard & Lupton (1998) advocate decomposing K into a linear combination of basis functions

$$K(u, v) = \sum_{k=1}^N \sum_{\substack{p,q=0 \\ p+q \leq M_k}} a_{pq} u^p v^q e^{-(u^2+v^2)/2\sigma_k^2}, \quad (2)$$

where a_{pq} are coefficients. The Gaussian widths σ_k and integers N and M_k control the complexity of the kernel shape. Similarly the differential background is modelled as a sum of polynomial basis functions:

$$B(x, y) = \sum_{r,s=0}^{r,r+s \leq M_b} a_{rs} x^r y^s, \quad (3)$$

where a_{rs} are coefficients and the integer M_b is the degree of polynomial used to model the differential background.

There are a number of freely available software implementations of the OIS algorithm, the best known of which are ISIS¹ and DIAPL². Throughout this paper we use ISIS version 2.2 (Alard & Lupton 1998; Alard 2000). However, we stress that the shortcomings we illustrate are not specific to ISIS but are shared by all implementations of OIS that assume simple polynomial forms for the differential background as in Equation (3). As pointed out in the review of Wozniak (2008) the OIS method is actually independent of the choice of basis function or even the use of basis functions at all. Bramich (2008) has implemented a version of OIS (DANDIA) in which Equation (1) is minimized pixel-by-pixel without assuming a particular form of basis function. This method solves for the kernel for an assumed constant background within a sub region. The global differential background solution is then found via interpolation over a grid of sub-regions. However for complex differential backgrounds of the kind investigated in this paper the method would potentially require splitting the image into a very large number sub-regions in the absence of prior knowledge on the shape of the differential background and its behaviour with respect to time.

¹ <http://www.iap.fr/users/alard/package.html>

² <http://users.camk.edu.pl/psych/DIAPL/>

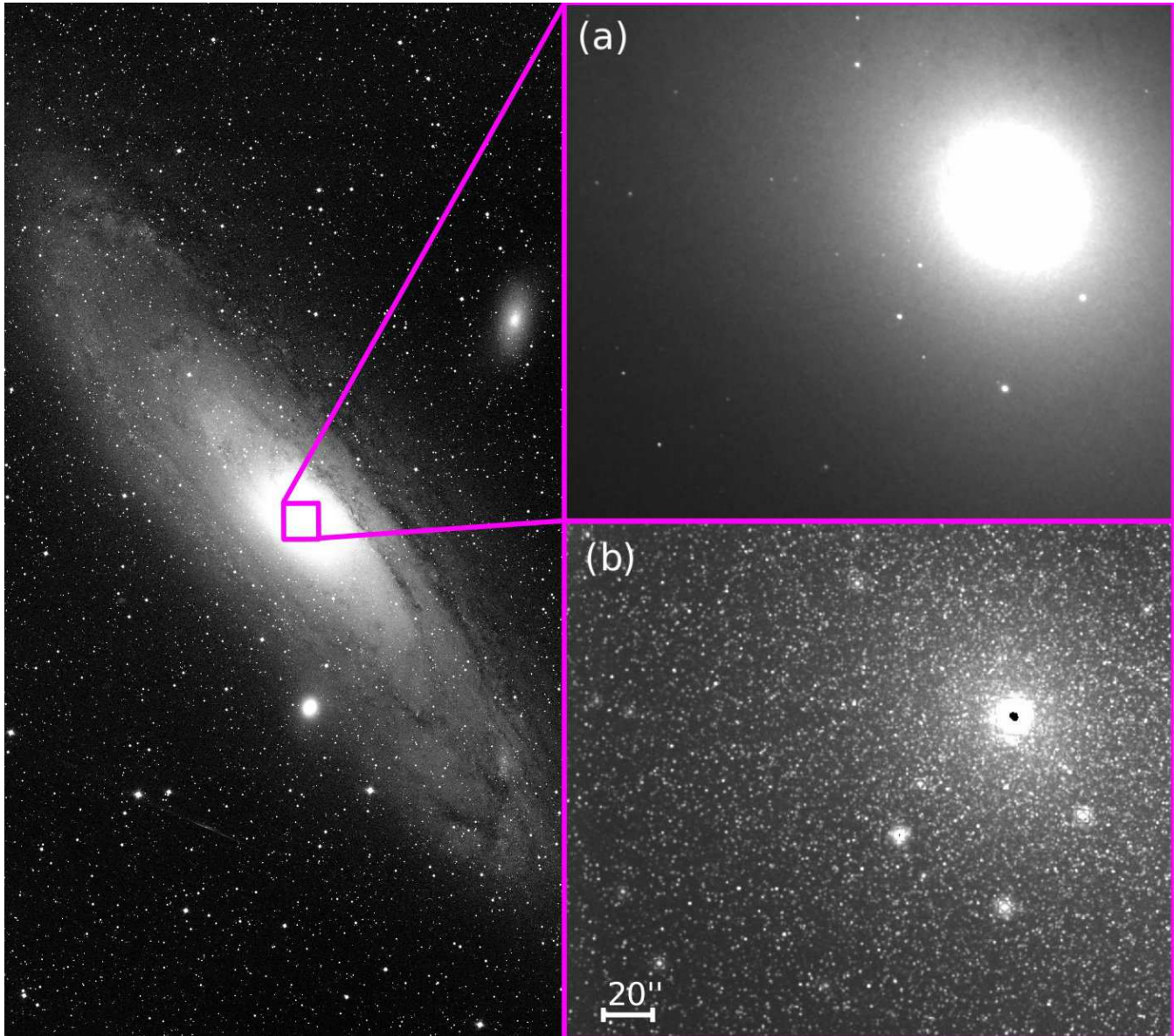


Figure 1. *Left panel:* The position of the Angstrom Project robotic field shown on an NOAO image of the Andromeda Galaxy (M31 - image credit: Bill Schoening, Vanessa Harvey/REU program/NOAO/AURA/NSF). *Right panels:* (a) A Sloan i' -band stacked image of the Angstrom Project robotic field obtained from the Liverpool Telescope at La Palma. This image is used as our reference image for the tests in this paper and covers the inner $\sim 4' \times 4'$ of the M31 bulge. (b) The locations of thousands of variable stars around the M31 core are revealed by combining a stack of 480 difference images. The difference images span 5 years and are created from a sequence of more than 3300 individual exposures. The difference images were created using the modified method described in this paper. Composite residuals from imperfect subtraction within the inner $\sim 10''$ of the core and around some bright foreground stars are also visible.

2.3 Difference imaging of Angstrom Project data

We have applied the OIS method to a series of Sloan i' -band images of the M31 bulge obtained by the Angstrom Project (Kerins et al. 2006) using the Liverpool Telescope (hereafter LT, Steele et al. 2004) on the Canary Islands. The Angstrom Project is undertaking long-term monitoring of the bulge of M31 in order to detect stellar microlensing events and transients. The survey employs a real-time difference imaging pipeline capable of issuing alerts of ongoing events (Darnley et al. 2007). The location of the Angstrom robotic telescope field is shown in Figure 1.

The LT is a 2m robotic telescope housing an optical camera (RATCAM) with a $4'.6 \times 4'.6$ field of view with $0'.13$ pixels. Im-

ages were obtained over a 5-year period from 2004–2009. The LT typically obtained one or two epochs of data per clear night during the M31 observing season (August–January) with each epoch comprising a run of between 7 and 15 short exposures, typically ranging from 30 to 200 seconds. The exposures were kept short to avoid saturation of the M31 core and bright foreground stars. Pre-processing, comprising de-biasing and flat fielding, was carried out by the LT robotic telescope pipeline. The Angstrom Project pipeline then performed preliminary geometric alignment and de-fringing, followed by optimal image alignment using Fourier cross correlation (for further details see Darnley et al. 2007).

All images were built by aligning and stacking individual im-

ages within each observing epoch to form a high signal-to-noise epoch frame. The master reference frame was constructed from a stack of 30 high quality individual exposures obtained over four separate epochs from the 2007/8 and 2008/9 observing seasons. These epochs were chosen on the basis of accurate telescope pointing and tracking, low airmass, low background levels and good seeing. ISIS can itself be used to build the reference image from a stack of high quality frames by matching their PSFs and background using Equation (1). We choose instead to create our reference frame by first photometrically aligning the selected images (using the method described in Section 3.1) and then median stacking them using the IRAF `IMCOMBINE` task. Hence our difference image results rest only on a single application of Equation (1) when matching the reference and target images. The same reference image is used throughout so that variations in our results depend only on how we manipulate the target frame. The reference frame is shown in panel (a) of Figure 1.

Figure 2 shows some example difference images created from the reference image and a very high quality target image obtained under excellent seeing. The results illustrate the challenge of accurate background matching towards the core of M31 where, even within the small LT field of view, the dynamic range in surface brightness across the image is around two orders of magnitude. In Figure 2(a) ISIS uses a second-order polynomial to model the differential background across the whole image area. Whilst the resulting difference image clearly succeeds in revealing a wealth of variable stars (evidenced by the black and white spots, which show sources that have dimmed or brightened) it suffers from a significant large-scale background residual. We find that the amplitude of the residual is largely insensitive to the choice of polynomial order, though the residual pattern across the image does vary according to the order used, as one would expect. The underlying differential background is therefore clearly not well represented by a 2D polynomial. This can be caused by flat field errors that scale with pixel flux, and therefore would be expected to have a distribution that varies as a function of the exponential surface brightness profile. Scattered light, internal reflections and dust can cause additional problems as can fringing effects. Often these effects are inadequately modelled by a polynomial function.

In fact the amplitude of the background variation over most of the image area in Figure 2(a) typically represents only $\lesssim 1\%$ of the original image flux, but this is still too large to allow reliable difference image photometry of sources, which themselves are varying at a level of a few percent of the background surface brightness flux. Since the residual background is epoch dependent the failure to effectively remove it means that robust relative photometry between epochs becomes virtually impossible. Additionally, the large-amplitude background residual may blunt the OIS algorithm's sensitivity to the optimal PSF transformation because the overall summed squared difference flux [D^2 in Equation (1)] can become dominated by the background residual rather than by PSF kernel residuals.

Whilst these effects are important for high surface brightness regions such as the M31 bulge they are far less important for Galactic surveys that employ difference imaging. Even towards the Galactic bulge the flux observed by optical surveys is dominated by resolved or semi-resolved stars and therefore any background residuals from systematic problems will be typically at a low level even on difference images. However, it is feasible that photometric corrections might benefit future near-infrared surveys of the Galactic bulge, which can target the centre of the Galaxy where the unresolved stellar background flux is considerably higher. Near-infrared

array technology is also still maturing and so is currently more prone to systematic problems than optical CCDs.

The ISIS software also provides the option of running the OIS algorithm independently within sub-regions of an image. In Figure 2(b) we show the difference image result where ISIS has split the image into 4×4 sub-regions. All other DIA parameters are the same as for Figure 2(a). This time ISIS does a better job over much of the image area. However, within the inner bulge region, covering around half the field area, noticeable background residuals are still evident, especially at the square sub-region boundaries, which show sharp discontinuity. One might be tempted to try to reduce the effect by further increasing the number of sub-regions. However, we are fundamentally limited by the size of the image stamps within which the convolution kernel is determined, which in turn is limited by the scale of the image PSF. For the image in Figure 2(b) each sub-region is only around 200 pixels wide, compared to a stamp width of 30 pixels. Ideally the PSF and background should be evaluated within several independent stamps across the sub-region in order to facilitate a good solution for the PSF transformation. The sub-regions also should be large enough to contain resolved or partially resolved stars, or strong features such as dust lanes, so that the solution to equation (1) is not dominated by noise.

3 A MODIFIED PROCEDURE FOR DIFFERENCE IMAGING

We have seen that ISIS may not yield optimal results when images are dominated by high background flux levels and contain systematics that scale with image flux. The core of the problem is that the OIS algorithm performs PSF and background flux matching simultaneously, whilst prior to OIS these were treated separately (Tomanev & Crofts 1996; Ansari et al. 1997), giving robust results towards high surface brightness targets such as M31. However the OIS algorithm provides improved photometric accuracy than earlier schemes due to its flexibility in modelling the PSF. Ideally we would like to combine the best of the old and current approaches.

To this end we choose to separate out the photometric and PSF matching stages, as in earlier approaches. Then we run ISIS with differential background matching effectively turned off by setting the background polynomial to order zero [i.e. setting $M_b = 0$ in Equation (3)]. In this case the least squares minimization of D^2 in Equation (1) should be driven by the quality of the PSF transformation kernel K rather than potentially having to trade between the quality of PSF and background matching.

3.1 Separating photometric and PSF matching

For the photometric matching we start by first determining a gross linear scaling between R and T using the `LINMATCH` task within IRAF³ to perform linear photometric matching within a common region covering around 40% of the total image area. This task assumes that the reference and target images are linearly related in their flux ($R = a \times T + b$). The scaling a and offset b are then applied to T to obtain a linearly photometrically matched image T_L . After linear scaling we subtract T_L from R to obtain a residual

³ IRAF is distributed by the National Optical Astronomy Observatories, which are operated by the Association of Universities for Research in Astronomy, Inc., under cooperative agreement with the National Science Foundation.

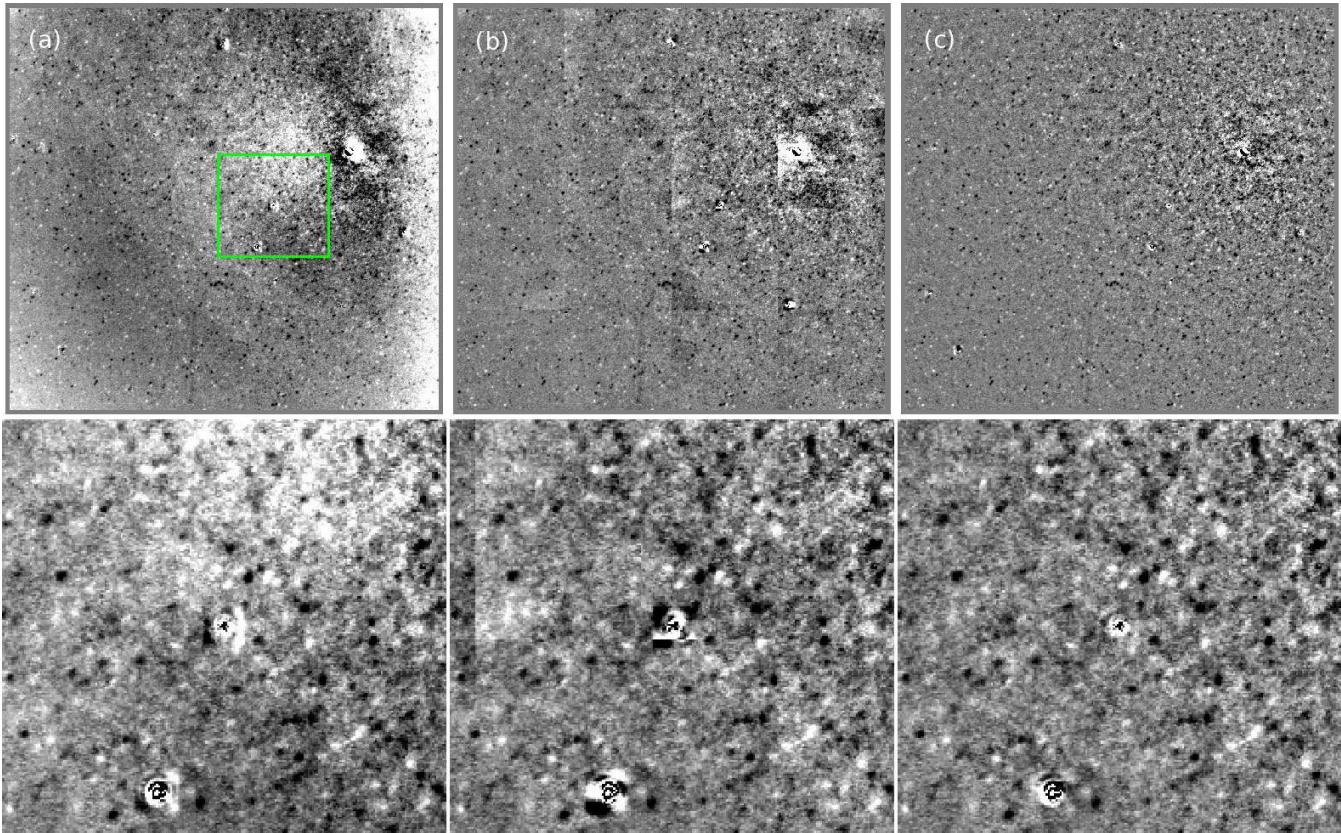


Figure 2. *Upper panels:* difference images produced by ISIS (version 2.2) from a pair of high quality reference and target images covering an area of $3'.9 \times 3'.7$ around the M31 core. In (a) ISIS is run on photometrically unaligned images allowing a second-order polynomial to model the differential background. Strong background residuals remain in the difference image, which do not markedly improve with the use of higher order polynomials. In (b) the photometrically unaligned images are split into 16 sub-regions on which ISIS is run individually using the same parameters as in (a). The background matching is better further out from the core (apparently at the expense of poorer PSF matching) but remains poor closer to the core where the boundaries between the sub-regions are evident. In (c) the images have been photometrically aligned using the method discussed in this paper, prior to running ISIS. In this case a zeroth-order polynomial has been imposed for the differential background when running ISIS. All other parameters are the same as in (a) and (b). *Lower panels:* show a $1' \times 0'.9$ zoom of the region shown by the box in (a) for each case (a), (b) and (c), respectively. In (c) note how the removal of the differential background also improves the quality of PSF matching as evidenced by the lessened residuals around bright foreground stars.

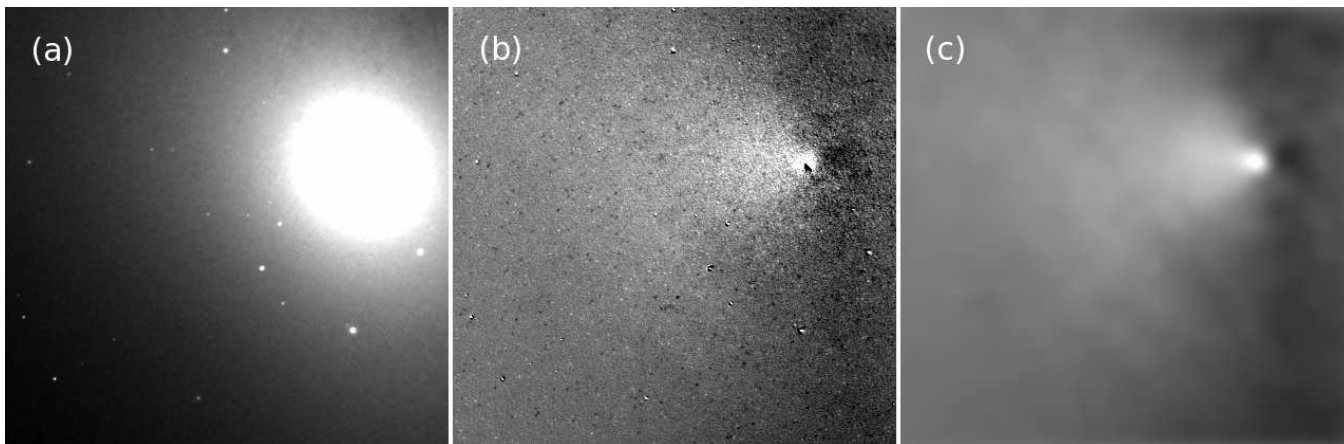


Figure 3. Matching the non-linear background residual. A target image (a) which has been linearly matched to the reference image [shown in Figure 1(a)] is directly subtracted from it to reveal a residual map (b). The map reveals a large scale non-linear variation in the residual background level. This map is then Gaussian filtered to produce a smoothed residual background map (c). The contrast level in (b) and (c) has been stretched by a factor 30 over that in (a) to highlight the background residual, which has an amplitude that is typically only about 1% of the target image flux. The smoothed residual map is added back on to the target image to produce the final photometrically corrected target frame. The difference image resulting from the corrected target frame is shown in Figure 2(c).

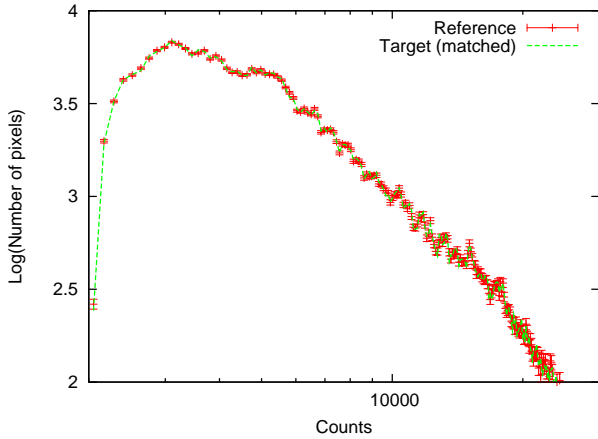


Figure 4. Flux count histograms of the reference image (points with errors) and target image (dashed line) after the target has been photometrically aligned to the reference. The pseudo errors on the reference image pixel numbers assume an expected Poisson-like variance in the pixel numbers between aligned images. After alignment the behaviour of the target count histogram accurately mirrors that of the reference image even down to small scale deviations.

image $R - T_L$. Since the seeing is generally different between R and T_L the differential flux from genuinely variable sources is significantly smoothed out by differences in image PSF. A Gaussian filter is then passed over the residual image to produce a smoothed residual background image B' . The size of the Gaussian is set to $\sigma = 15$ pixels, which is large enough to be insensitive to the presence of variable stars but small enough to provide a good local estimate of the differential background. Finally a background corrected target image $T' = T_L + B'$ is obtained. Figure 3 illustrates how the differential background map B' is produced from a target image which has already been linearly matched to the reference frame.

Figure 4 shows the resulting pixel flux histograms after photometric matching. Normally, good photometric alignment between images requires that the PSFs are matched first. However around the M31 bulge the image flux is dominated almost everywhere by the smooth unresolved surface brightness distribution, so the photometric calibration is insensitive to seeing and we obtain very good photometric alignment.

The adjusted image T' now has a background that is properly matched to R so that ISIS can be run without the inclusion of the B term in Equation (1).

The result of running ISIS on a target image that is now photometrically aligned to the reference frame is shown in Figure 2(c). All ISIS configuration parameters are set the same as for the previous tests in Figure 2(a) and (b) except we now enforce a zeroth-order polynomial model for the differential background. The resulting difference image is clearly superior to the previous examples. There is now no noticeable background residual anywhere on the image. Equally important is the fact that the PSF transformation is clearly much improved too. This is evident when examining the residuals associated with the few bright foreground stars visible within the Angstrom field (compare with the reference image shown in Figure 1). These foreground stars leave relatively strong residuals in the difference images shown in Figure 2(a) and (b) but they are much reduced in Figure 2(c) (see also the zoomed inset panels). This indicates that ISIS has been able to find a better PSF

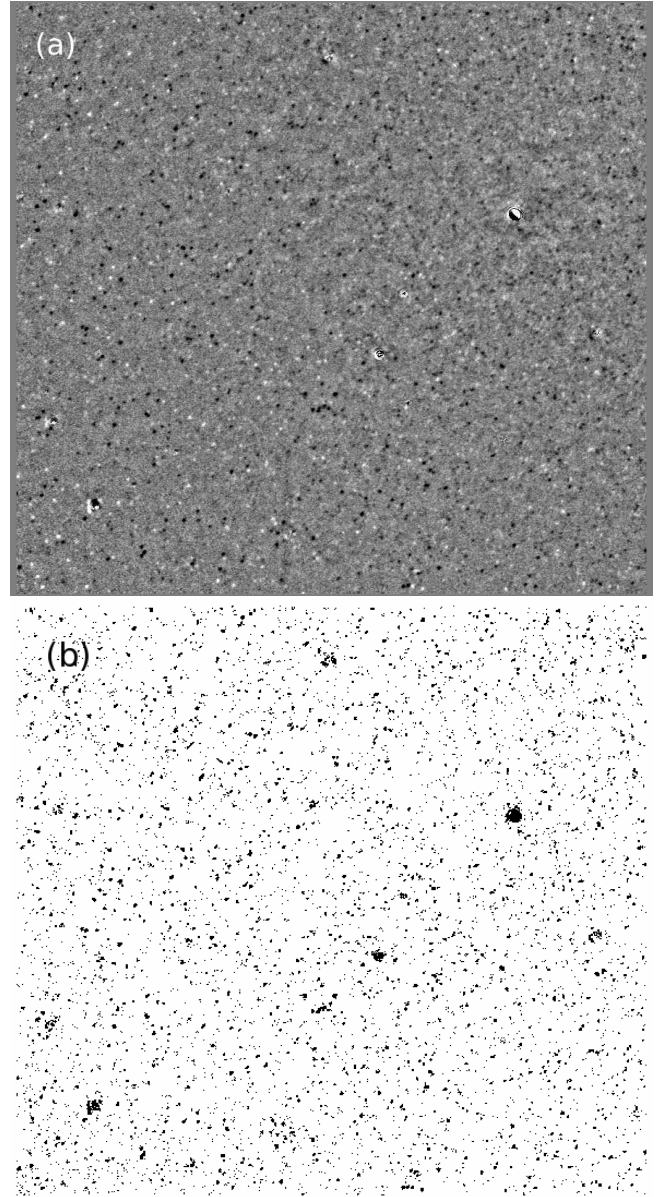


Figure 5. (a) Grey-scale “signal-to-noise” map produced by dividing the difference image shown in Figure 2(c) by the square root of the combined reference and target image counts. Note how the increase in image noise towards the M31 core suppresses the number of detectable variations there, though some are still evident to within $\sim 10''$ of the core. (b) A map of all the pixels in (a) that exceed 2.5σ . Isolated pixels are rare and most belong to PSF-like clusters that are associated with genuinely variable objects. These provide the excess seen in the tails of the noise histogram shown in Figure 6.

solution as a result of minimizing Equation (1) for photometrically aligned images.

Figure 5(a) shows a map of the signal to noise (S/N) ratio. The signal-to-noise map is defined by

$$S/N = \frac{\sqrt{gMN}(R - T)}{\sqrt{MT + NR}}, \quad (4)$$

where M is the number of individual exposures comprising the target frame stack T , N is the number of individual exposures comprising the reference stack R and g is the CCD gain. The grey-scale

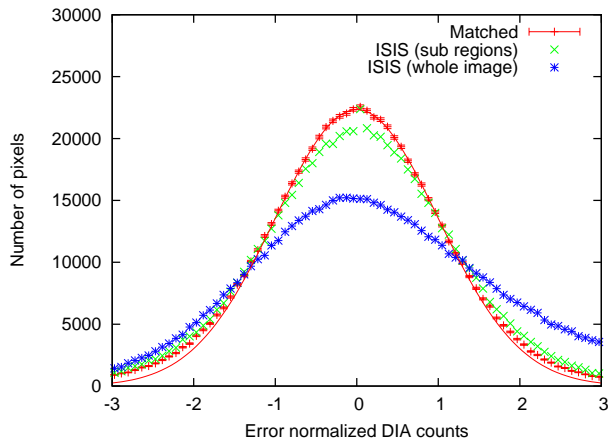


Figure 6. Histogram of the counts for the image shown in Figure 5(a) together with the best-fitting Gaussian. The fit is performed within $\pm 1 \sigma$. The excess from pure Gaussian noise evident in the tails of the histogram is predominately associated with genuinely variable objects as shown in Figure 5(b). Also shown are the equivalent histograms for the difference images shown in Figure 2(a) and (b) where no photometric alignment is performed prior to running ISIS.

in Figure 5(a) is calibrated to show pixels with $|S/N| > 10$ as either white or black depending upon whether the difference flux is positive or negative. The main difference in the appearance of this S/N image with the corresponding difference image shown in Figure 2(c) is that near the M31 core the S/N image shows much less variation, indicating that many of the flux deviations on the difference image near the M31 core are just due to the noise arising from the very high surface brightness level. Figure 6 shows the resulting pixel histogram of S/N values, together with the best fitting Gaussian model within $\pm 1 \sigma$. The histogram shows that within this region the noise is well approximated as Gaussian. The tails of the distribution exhibit an excess over and above Gaussian noise. However most of these pixels are associated with genuinely varying objects, which from Figure 5(b) clearly make up a non-negligible fraction of the image pixels. Figures 5 and 6 therefore suggest that photometrically aligned images can allow high quality difference imaging even to within a few arcseconds of the M31 bulge.

In Figure 7 we show two periodic variable star light-curves from the Angstrom Project data. The top panels show the light-curves produced by ISIS without initial photometric alignment of the images. The lower panels show the result of running ISIS on the images after photometric alignment. For fair comparison we have not rejected outlier data points so the light-curves include some data from relatively poor quality images that might normally be rejected through a quality control cut. Whilst periodic behaviour is recognisable in the top panels the photometry is clearly more erratic than for the photometrically aligned versions in the lower panels. The variable in the right hand example is rather noisier than the one on the left but this is because it is located just $9''$ from the M31 core, corresponding to a projected distance of 35 pc at the distance of M31. Here the the surface brightness levels are extremely high and so we expect the light-curves to be much noisier.

It is noticeable that the first season of Angstrom data shows good consistency with subsequent seasons for the variable star shown in the left-hand panels of Figure 7, which is located $2'.3$ from the M31 core (about a half of the LT field width away). However

the light-curve of the variable close to the M31 core shown in the right-hand panels is much more erratic during the first season than in subsequent seasons. Visual inspection of the images shows that the majority of images taken during the LT commissioning season in 2004 show evidence of scattered or reflected light close to the core (c.f. Figure 8 in Section 4.1). This is substantially reduced but not eliminated by the photometric alignment. Fortunately relatively few exposures in the subsequent observing seasons are affected to the same level.

As Figure 5 shows, there are relatively few variable objects that are detectable above the noise so close to the M31 core but the example in Figure 7 demonstrates that, where they are detectable, we are usually able to obtain reliable photometry even in this extreme high-background regime.

4 THE ROBUSTNESS OF DIFFERENCE IMAGING

In this section we illustrate how photometric alignment of images prior to difference imaging can significantly lessen the effect of scattered or internally reflected light. We also show in Section 4.2 that difference imaging yields remarkably consistent results even when the sky density of variable sources is so high that it approaches the confusion limit.

4.1 Background light systematics

The photometric alignment procedure described in Section 3.1 can help alleviate some of the worst effects of systematics such as scattered or reflected light. As an example we selected an i' -band image stack obtained on LT in October 2004 [Figure 8(a)], not long after LT was commissioned, which appears to have excellent image quality but whose difference image [Figure 8(b)] reveals blotchy background residuals around the M31 core. This epoch appears to have suffered from the effects of internal reflection, where some of the light has reflected off the CCD and then reflected back again by reflecting surfaces in the telescope, resulting in faint ghost images of the M31 core that are not perceptible on the original frames but show up clearly on the difference image.

In order to minimize such effects we applied the photometric matching technique described in Section 3.1. We then ran ISIS on the modified target image to produce the difference image shown in Figure 8(c). This image shows a substantial reduction in the effects of scattered light, though it does not completely eliminate it in the vicinity of the M31 core.

In general, separating out the photometric and PSF matching parts of the OIS procedure allow for more complex bespoke treatments of the differential background and therefore, in principle, should yield results closer to optimal difference image photometry.

4.2 The effect of variables

The high crowding levels of genuinely variable sources evident in Figure 2 potentially poses a problem for the OIS algorithm. The minimization in Equation (1) would be expected to correspond to the optimal difference image only in the limit that, in the absence of seeing and background variations, most of the image flux does not vary with time. In theory it could be the case that the relative phases and amplitudes of variables within a stamp at a given epoch could pose a significant source of time variability in the average difference flux within the stamp. If so this could affect the residual background model determination.

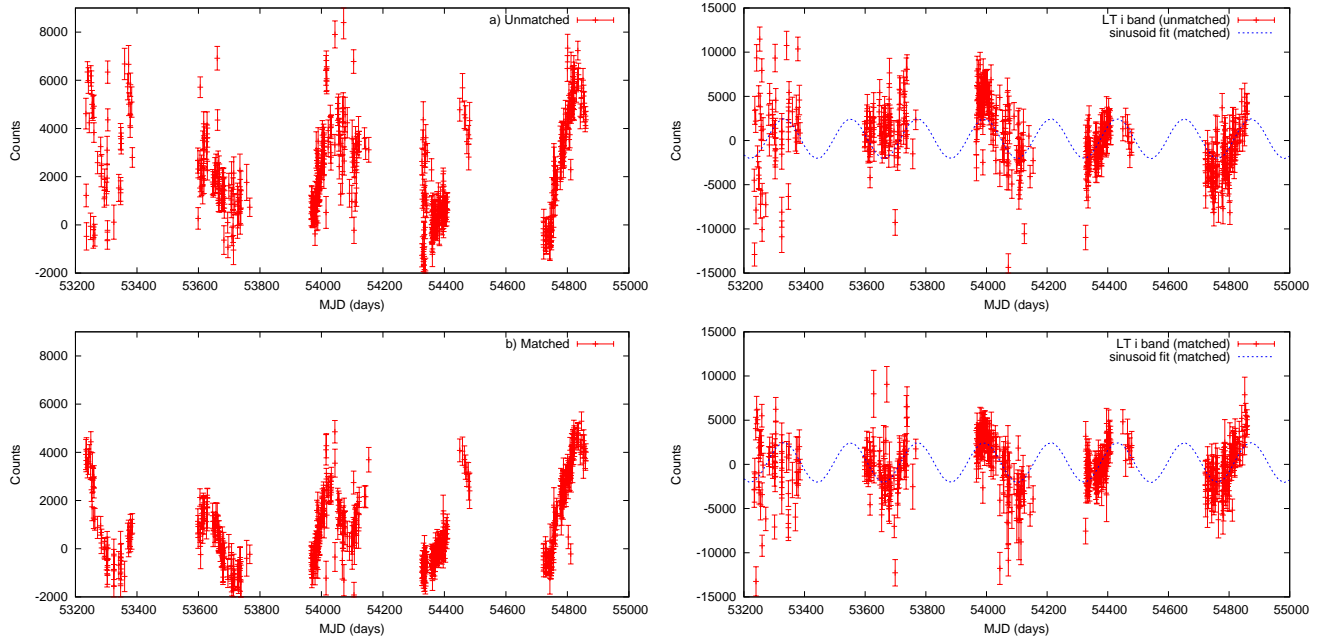


Figure 7. *Left:* Full five season LT i' -band light-curves of a periodic variable star from ISIS applied to (a) photometrically unaligned images and (b) photometrically aligned images. The variable is located $2.3''$ from the M31 core. *Right:* a light-curve showing a periodic variable located just $9''$ from the M31 core, corresponding to a projected distance of 35 pc at the distance of M31. The top panel shows the DIA light-curve from photometrically unaligned data and the lower light-curve is from aligned data. A simple sinusoid with a period of 220 days has been fitted to the aligned data in the lower panel and it is also shown in the upper panel for comparison. No selection has been performed to remove outliers.

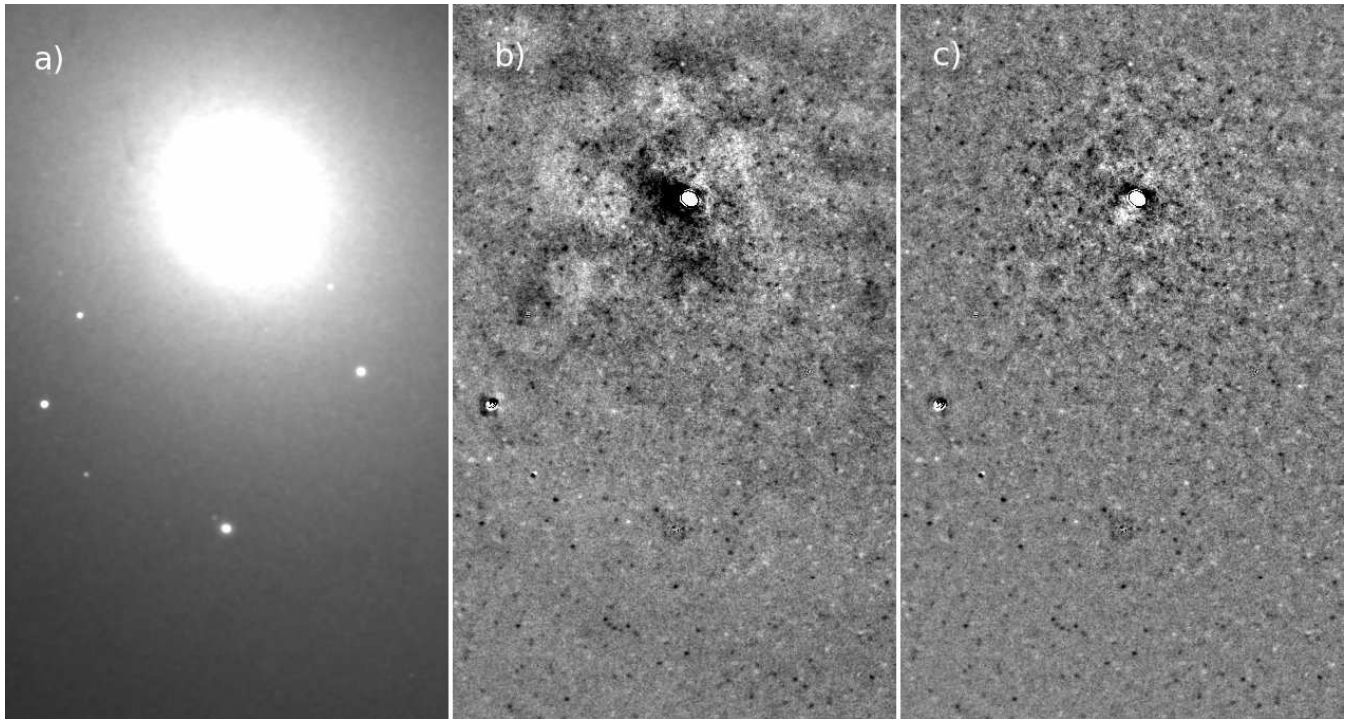


Figure 8. Photometric alignment can help to substantially reduce undesirable systematics, such as internal reflections. In (b) the result of differencing the target image shown in (a) reveals strong reflected light residuals around the M31 core. In (c) the target image has been photometrically aligned to the reference prior to running ISIS (see Section 3.1), resulting in a significant reduction in the effects of internally reflected light.

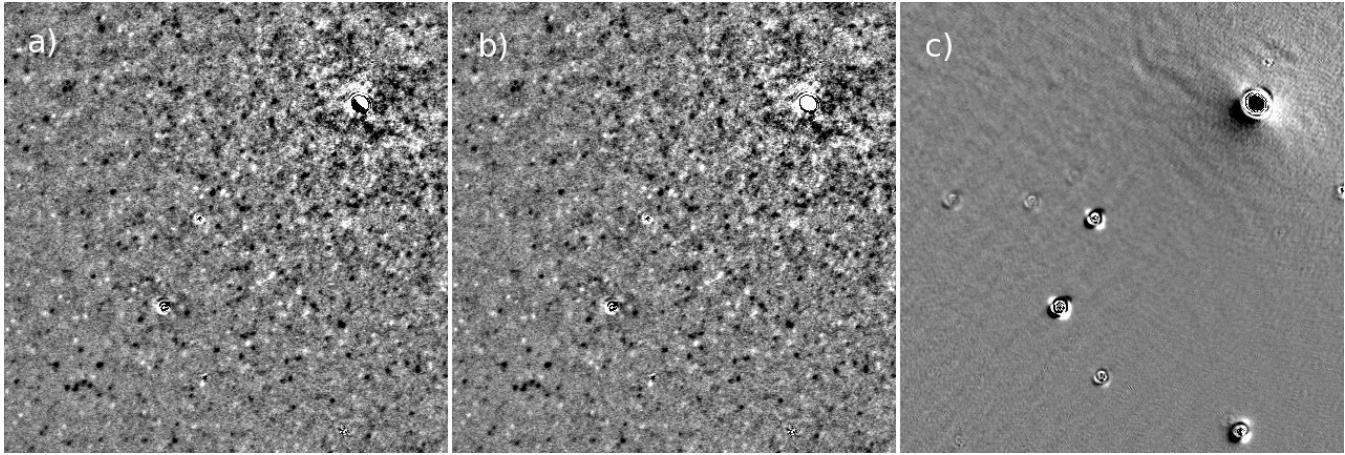


Figure 9. The effect of variables on the computed DIA kernel. The difference image in (a) is computed from photometrically matched images using ISIS. In (b) we have employed a double-pass algorithm described in the main text, which minimizes the sensitivity of the kernel solution to the presence of variables. In (c) we show the difference between (a) and (b), with the grey-scale in (c) set to a contrast level that is 20 times higher than in (a) and (b) to emphasize any discrepancies. Despite the high density of variables in the image there is very little variation between the two difference images.

In fact Figure 5 indicates that the high sky density of variable stars is not responsible for the poor quality difference image presented in Figure 2(a) and (b). Whilst ISIS performs worst in the vicinity of the M31 core the S/N map shown in Figure 5(a), derived from photometrically aligned images, shows that the number density of detectable variables actually drops close to the M31 core due to the high photon noise from the central M31 surface brightness flux. Nonetheless whilst variables are not the cause of the differential background residual it is not clear that Equation 1 will yield the same or similar kernel solution as it would in the absence of intrinsically variable sources, so it is prudent to test this.

In order to assess the validity of OIS within such a crowded variable source regime as the M31 core we have adapted the OIS implementation within ISIS to perform a double-pass iterative minimization of Equation (1) that is less sensitive to the presence of variable sources. On the first pass the algorithm runs in the normal way. Then all pixel fluxes on the resulting difference image above a specified absolute flux threshold are added back on to the target frame to form a modified target image in which intrinsically variable sources are largely removed (i.e. matched to their flux values on the reference image). A second pass of OIS is then performed on this modified target frame. The resulting kernel solution for the modified frame is then applied to the reference image and the convolved reference is subtracted from the original (unmodified) target frame to create the final difference image. This method ensures that the final difference is largely insensitive to the presence of variable stars.

Figure 9 compares the result of a standard difference image created with ISIS [from photometrically aligned images – panel (a)] with the result using the double-pass procedure described above [panel (b)]. Panel (c) shows the difference between the two difference images, though the grey-scale contrast in (c) has been increased by a factor 20 over (a) and (b) to highlight any deviation. In fact the two results are virtually identical over most of the image area, showing that ISIS is capable of finding an optimal kernel solution even for high crowding densities of variable stars.

5 DISCUSSION

In this paper we have shown that optimal difference imaging in regions of very high background levels, such as the bulge regions of galaxies, can be severely compromised due to the presence of systematics that scale with the image flux, such as internal reflections, scattered light, flat field errors or fringe effects. In these cases difference images created using the Optimal Image Subtraction (OIS) algorithm (Alard & Lupton 1998; Alard 2000), which is the most widely used difference image algorithm, may exhibit large amplitude background residuals that make reliable relative photometry difficult if not impossible. Fortunately, we have shown that OIS is able to give very good results provided the images to be differenced are first photometrically aligned prior to difference imaging.

Using the photometric alignment procedure we find we can produce difference images of the M31 bulge that are close to photon noise limited even within a few arcseconds of the M31 nucleus. Not only does this minimize or eliminate large amplitude background residuals but it also noticeably improves the quality of the PSF kernel transformation. We have also shown that despite the fact that the sky density of variable stars in the M31 bulge is approaching the confusion limit, difference imaging is able to provide robust photometry in this regime.

The problem we highlight is specific to targets in which the background brightness is high. The OIS method is well known to cope admirably for stellar fields within our Galaxy, as imaged by current optical surveys, where the image flux is dominated by resolved or semi-resolved stars rather than by the diffuse background light. However, future near-infrared time-domain surveys of the Galactic Centre could also conceivably benefit from a separation of the photometric and kernel matching stages.

ACKNOWLEDGEMENTS

JPD was supported by a PhD studentship from the UK Science and Technology Facilities Council (STFC). This work was supported by the research grant of the Chungbuk National University in 2009. The Liverpool Telescope is operated on the island of La Palma by Liverpool John Moores University in the Spanish Observatorio del

Roque de los Muchachos of the Instituto de Astrofísica de Canarias with financial support from STFC.

REFERENCES

- Alard, C. & Lupton, R., 1998, *ApJ*, 503, 325
Ansari R., et al., 1997, *A&A*, 324, 843
Alard, C. 2000, *A&AS*, 144, 363
Bramich, D. M. 2008, *MNRAS*, 386, L77
Darnley, M. J., et al. 2007, *ApJ*, 661, L45
Kerins, E., Darnley, M. J., Duke, J. P., Gould, A., Han, C., Jeon, Y.-B., Newsam, A., & Park, B.-G. 2006, *MNRAS*, 365, 1099
Steele I. A., et al., 2004, *SPIE*, 5489, 679
Tomaney, A. B., & Crotts, A. P. S. 1996, *AJ*, 112, 2872
Wozniak, P. 2008, Manchester Microlensing Conference, eds E. Kerins, S. Mao, N. Rattenbury and L. Wyrzykowski, Published online at SISSA, Proceedings of Science, p.3